

RECEPTIVE PROFILES INDUCE FUNCTIONAL ARCHITECTURE OF V1

NOEMI MONTOBBIO, GIOVANNA CITTI, AND ALESSANDRO SARTI

ABSTRACT. In this work we show how to construct connectivity kernels induced by the receptive profiles of simple cells of the primary visual cortex (V1). These kernels are directly defined by the shape of such profiles: this provides a metric model for the functional architecture of V1, whose global geometry is determined by the reciprocal interactions between local elements. Our construction adapts to any bank of filters chosen to represent the set of receptive profiles of simple cells, since it does not require any structure on the parameterization on the family. The connectivity kernel that we define carries a geometrical structure consistent with the well-known properties of long-range horizontal connections in V1, and it is compatible with the perceptual rules synthesized by the concept of association field. These characteristics are still present when the kernel is constructed from a bank of filters arising from an unsupervised learning algorithm.

1. INTRODUCTION

The primary visual cortex (V1) implements the first stage of cortical processing of the visual information, and it is the most studied and the best understood among the visual areas in the brain. An essential concept related to the structure of V1 is that of *receptive profile* (RP), i.e. the function modeling the impulsive response of a neuron. Indeed, the primary step of computation taking place in V1 involves a class of neurons, called *simple cells*, which act approximately as linear filters on the retinal image. In other words, the action of such a neuron on a visual stimulus can be expressed, to a first approximation, as the convolution between the image and the RP of the cell.

A classical model for the set of receptive profiles of V1 simple cells is provided by a bank of bidimensional Gabor filters ([17], [9], [19]). Such a family can be indexed by a set of parameters showing a group structure: this fact is at the basis of a number of models, which identify the set of simple cells with such space of parameters and define on it a differential structure, designed to be compatible with the above-mentioned group law ([26], [8], [30]). This idea can in principle be replicated as long as the bank of filters modeling the RPs can be parameterized by a group. Yet, this condition is not verified if one considers for example a bank of filters learned through automatic learning procedures (see e.g. [24], [2]). It is nonetheless crucial for a cortex model to describe the *functional architecture* ruling the geometry of intra-cortical connections: these are indeed thought to be responsible for the integration of local features into contours, shapes, objects. Specifically, the contextual influences modulating V1 neurons' activity have been described through the concept of *association field* [11], which specifies the geometrical properties of the influences between neurons even with markedly separated RPs, based on their reciprocal position and orientation. The long-range, orientation specific horizontal connections which are known to take place in V1 are believed to be at the basis of such mechanisms of perceptual grouping [4].

The aim of this paper is to show that a bank of receptive profiles can induce such a functional architecture, with or without the presence of a group structure. We propose to express the connectivity strength through a kernel defined onto the family of

RPs and generated by the RPs themselves. Specifically, we consider a bank of filters $\{\psi_p\}_{p \in \mathcal{G}} \subseteq L^2(\mathbb{R}^2)$, where \mathcal{G} is any set of parameters indexing the family. As in [8], we identify each filter ψ_p with the corresponding index $p \in \mathcal{G}$. We shall refer to \mathcal{G} as the *feature space*: intuitively, one may think that each element $p \in \mathcal{G}$ encodes the features extracted by the corresponding filter ψ_p when it is applied to some image. We then define, for each couple of points $p, p_0 \in \mathcal{G}$, the *generator*

$$K(p, p_0) := \operatorname{Re} \left(\int_{\mathbb{R}^2} \psi_p(x, y) \overline{\psi_{p_0}(x, y)} dx dy \right),$$

i.e. $K(p, p_0)$ is defined to be the real part of the L^2 scalar product between the filters ψ_p and ψ_{p_0} . This kernel allows to define a natural metric structure on the feature space. We then construct, through an iterative mechanism of repeated integrations against K , a wider connectivity kernel from which we are also able to recover association-field-like patterns. Such a construction suggests that *the geometry of the horizontal connections in V1 can indeed be obtained from the shape of the receptive profiles*.

In the last part of the paper, we present some numerical simulations to demonstrate the applicability of our model to both the classical framework of a family of Gabor filters (including a spatiotemporal example), and the situation where the RPs of simple cells are represented by a bank of filters obtained through an unsupervised learning algorithm.

2. THE FUNCTIONAL ARCHITECTURE OF V1

In this section we first recall the basic notions of receptive field and receptive profile of a visual neuron, with a particular focus on V1. We then review the link between the mechanisms of perceptual grouping and the neural circuitry of horizontal connections in V1. Lastly, we briefly outline the main concepts underlying some existing cortex models based on differential structures.

2.1. Receptive fields and receptive profiles. Every subcortical or cortical neuron is linked, through the connectivity of retino-geniculo-cortical pathways, to a local domain D of the retina, called the *receptive field* (RF) of the cell. The *receptive profile* (RP) of a visual cell is a function $\psi(x, y)$ defined on D , measuring quantitatively the impulsive response of the neuron. Certain classes of cells act approximately as *linear filters* on the optic signal, meaning that their receptive profile provides, up to a first approximation, the necessary information to measure their reaction to a general stimulus (expressed as a function $I(x, y)$ of the retinal coordinates): this is indeed given by a *convolution*

$$\int_D I(x, y) \psi(x - x_0, y - y_0) dx dy.$$

Here, the RP is expressed in local coordinates around (x_0, y_0) , the retinal location around which it is concentrated: that is, the response of the cell at (x_0, y_0) is given by $\psi(0, 0)$.

As for gangliar cells in the retina, as well as LGN cells, it is a classic result of neurophysiology that their isotropic RPs are best modeled as Laplacians of Gaussians. Unlike the retinal and LGN cells, neurons with strongly anisotropic RPs can be found in V1.

2.2. The structure of V1. Let us now focus on the structure of the first of the visual cortical areas. V1 neurons can be divided into two main classes, as first discovered by Hubel and Wiesel in 1962 [15]: these are called *simple* and *complex* cells.

Simple cells are the first neurons in the visual pathway which are sensitive to orientation. The basic structure of their RPs consists of two to five tapering rows of alternating excitatory and inhibitory subregions [9]: it is presumed that each simple receptive field arises from multiple

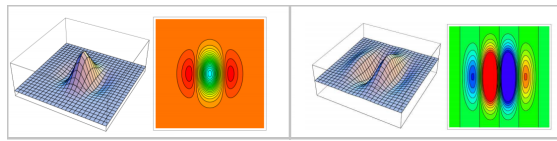


FIGURE 2.1. Two examples of RPs of simple cells of V1. Source: [25].

LGN receptive fields converging in a line [16]. Two examples of such profiles are shown in Figure 2.1. As already mentioned, the responses of simple cells display orientation and positional selectivity: each of them fires at an optimal orientation, giving progressively weaker responses as the orientation of the stimulus shifts sub-optimally. This behaviour is classically described by modeling the RPs of this class of cells through a family of *Gabor filters*, defined as complex exponential functions modulated by bidimensional Gaussian functions ([17], [9], [19]). The filters vary in retinal position, orientation and scale in order to describe the whole set of profiles. Starting from the basic filter

$$(2.1) \quad \psi_{0,0,0,1}(u, v) = \exp\left(\frac{2\pi i u}{\lambda}\right) \exp\left(-\frac{u^2 + v^2}{2\sigma^2}\right),$$

one can obtain the whole bank by translations, rotations and dilations. These are expressed by the following parameters: $(x, y) \in \mathbb{R}^2$ represents the position at which the filter is translated, $\theta \in S^1$ is the angle of the rotation and $\sigma > 0$ is the factor of dilation. Each combination of these transformations determine a filter $\psi_{x,y,\theta,\sigma}$ indexed by such parameters.

A different kind of processing is carried on by complex cells: unlike simple cells, their response cannot be explained through the linear action of a receptive profile on an image. These cells still display orientation sensitivity, but are *phase invariant*, i.e. they respond equally to optimally oriented bars independent of where they are placed inside the RF. A number of findings (see [20] for a review) led many authors to model the response of a complex cell as a square sum of simple cells with similar orientation and scale but with phases that differed in 90 degrees. Such a couple of cells is commonly referred to as a *quadrature pair*. This characterization of the development of phase invariance in complex cells is often called *energy model*.

However, the interactions between V1 neurons are not limited to the classical hierarchy of simple - to - complex cells. Indeed, there exist two main types of intracortical connectivity

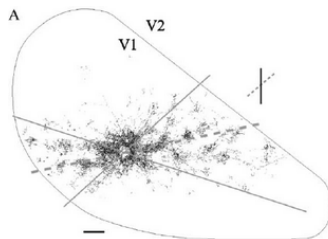


FIGURE 2.2. The horizontal connections departing from a pyramidal neuron of V1 layer 2/3 extend along an axis according to the preferential orientation of the cell. Source: [4].

affecting the responses of V1 neurons. Short-range connections, linking neurons whose RPs have the same retinal position but different orientations, act by selecting the orientation causing the maximal response to a stimulus and suppressing the others. On the other hand, lateral (or “horizontal”) connections associate neurons sharing the same preferred orientation, but linked

to different positions on the retina. The qualitative and quantitative properties of the latter have been investigated in several neurophysiological experiments, the best known of which are the ones performed by W. Bosking in 1997 [4] (see Figure 2.2): these connections show a marked orientation specificity and spread for millimeters horizontally along the cortex, linking cells whose receptive fields do not overlap. Such attributes make them a likely candidate to account for the processes of perceptual grouping carried on by our visual system.

2.3. Contextual influences and association fields. The human visual system is highly efficient in detecting and segregating objects. One of the main aspects in the perception of shapes is the identification of contours: this cannot be explained through the classical concept of receptive field ([14], [23], [1]), which refers to the extraction of *local* image features from the visual scene. In other words, the activity of cells is not only influenced by inputs within their RF, but rather it strongly depends on the context.

As far as V1 is concerned, it has been proposed (Field, Hayes and Hess, 1993 [11]) that the

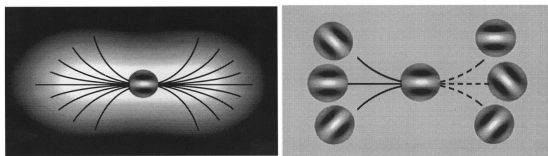


FIGURE 2.3. Source: [11].

interaction of local edge elements in this area can be described through an *association field*, consisting of a region around each V1 cell where the activation of other neurons characterized by certain preferred orientations tends to be enhanced by the excitation of the central cell. See Figure 2.3, from the original 1993 work of Field, Hayes and Hess. A number of psychophysical experiments, described in [11], suggested that the area covered by this activation region around a neuron is considerably wider than the receptive field of the cell.

In this case, the interactions mediated by the association field show facilitatory influences for neurons whose receptive fields have a similar preferred orientation; however, there may exist an analogue entity in other cortical areas [13], which links neurons sharing different and more abstract features. In other terms, each area could be endowed with an *intrinsic* correlation kernel, closely linked to the type of analysis performed in it, yielding corresponding perceptual patterns.

As just mentioned, the association field observed in V1 is believed to be intrinsic to this area: a possible anatomical framework is represented by the long-range horizontal connections ([26], [12]), as they fittingly link neurons with widely separated receptive fields whose reciprocal orientations are colinear or co-circular.

2.4. Previous models. Neuromathematical models of V1 typically adopt a differential approach to modeling the functional architecture of this area. In [8], the action of a bank of Gabor filters on a visual stimulus is shown to naturally induce a sub-Riemannian structure on the Lie group $\mathbb{R}^2 \times S^1$. In particular, consider a Gabor function

$$\Psi(x, y, \theta) = \exp\left(-\frac{\xi^2 + \nu^2}{\sigma^2}\right) \exp\left(i\frac{\nu}{\sigma^2}\right),$$

where

$$\xi = x \cos \theta + y \sin \theta, \quad \nu = -x \sin \theta + y \cos \theta.$$

The outcome of filtering an image I with Ψ can be locally approximated as

$$(2.2) \quad O(x, y, \theta) = X_3 \exp\left(-\frac{\xi^2 + \nu^2}{\sigma^2}\right) * I =: X_3 I_\sigma,$$

where

$$(2.3) \quad X_3 = X_3(\theta) = -\sin \theta \partial_x + \cos \theta \partial_y.$$

I_σ is a smoothed version of I , obtained by convolving it with a Gaussian kernel.

This procedure *lifts* the 2D image domain to the 3D space $\mathbb{R}^2 \times S^1$: each point $(x, y) \in \mathbb{R}^2$ is sent to the point $(x, y, \bar{\theta}) \in \mathbb{R}^2 \times S^1$ s.t.

$$(2.4) \quad \bar{\theta} = \max_{\theta} O(x, y, \theta).$$

This “non-maximal suppression” principle is based on experimental evidence on the sharp orientation tuning of V1 neurons (see also [5], [6]). The selection of a direction X_3 defines at each point a subspace of dimension 2 of the Euclidean tangent space to $\mathbb{R}^2 \times S^1$, generated by

$$X_1 = \cos \theta \partial_x + \sin \theta \partial_y, \quad X_2 = \partial_\theta.$$

The planes generated by X_1 and X_2 at each point are called *horizontal planes* and determine a bracket-generating distribution on $\mathbb{R}^2 \times S^1$, thus defining a sub-Riemannian structure on it. In particular one has

$$(2.5) \quad [X_1, X_2] = -X_3,$$

so that the Lie algebra generated by X_1 and X_2 is the whole three-dimensional tangent space at every point. This property implies, thanks to the Chow Theorem, that any two points (x_0, y_0, θ_0) and (x, y, θ) of $\mathbb{R}^2 \times S^1$ can be connected through an integral curve of $X_1 + kX_2$, where k varies in \mathbb{R} . Such curves are called *horizontal curves*.

Just as the anatomical mechanism of horizontal connections is proposed to implement the

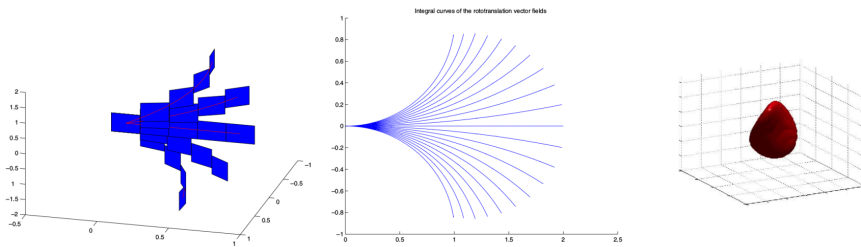


FIGURE 2.4. Left: integral curves of $X_1 + kX_2$ for varying values of k , visualized in $\mathbb{R}^2 \times S^1$, with contact planes displayed. Middle: their projection onto the image plane. Source: [8]. Right: a level set of the fundamental solution of the sub-Riemannian Laplacian.

perceptual association fields, the connectivity defined by this sub-Riemannian structure allows to recover such a pattern: the family of horizontal curves starting at a point (x_0, y_0, θ_0) can be interpreted as the local association field spreading from (x_0, y_0, θ_0) . See Figure 2.4 (left and middle). An extension of this model in the context of spatio-temporal analysis of visual stimuli was also developed in [3].

The propagation of neural activity in this sub-Riemannian space can be modeled by means of a diffusion equation expressed through second order operators defined in terms of the vector fields X_1 and X_2 . In [8], the heat equation associated to the sub-Riemannian Laplacian $\Delta u = X_1^2 u + X_2^2 u$ is considered. On the other hand, in [28] a statistical analysis of edge co-occurrence in a database of natural images led to considering a Fokker-Planck equation instead (see also [22], [29]). This corresponds to assuming that the propagation has a deterministic

component along X_1 and a stochastic component in direction X_2 . However, we will not address this kind of issue in this paper, where we will focus on a propagation more similar to the one introduced in [8]. Figure 2.4 (right) displays a level set of the fundamental solution to the sub-Riemannian Laplacian operator.

In the next sections, we will propose a new model of the functional architecture of V1 that does not need all differential structures of previous models. It is based on a metric structure on a suitable *feature space* indexing the RPs of simple cells. Such a geometry is induced by the RPs themselves. Interestingly, when the family of RPs is represented by a bank of Gabor filters indexed by $\mathbb{R}^2 \times S^1$, the induced distance is locally equivalent [21] to a Riemannian approximation to the sub-Riemannian structure described above. However, our model can be applied to a wide range of filter banks, with no need for any group structure, and is able to recover the perceptual rules of association fields even when applied to a randomly ordered family of learned orientation-selective filters.

3. A FUNCTIONAL ARCHITECTURE GENERATED BY RPS

3.1. The generating kernel. We fix a bank of linear real- or complex-valued filters on the plane, modeling the set of RPs of simple cells of V1. Specifically, we consider a family $\{\psi_p\}_{p \in \mathcal{G}} \subseteq L^2(\mathbb{R}^2)$, indexed by a *feature space* \mathcal{G} . These can be taken to be Gabor filters as well as any other bank of filters, for instance obtained through automatic learning procedures or to fit the shape of a set of experimentally measured RPs. Typically, the feature space has the form $\mathcal{G} = \mathbb{R}^2 \times \mathcal{F}$, where $(x, y) \in \mathbb{R}^2$ represents the retinal position at which the filter is centered and $f \in \mathcal{F}$ encodes the other features detected by the filters. Let us define, for every $p, p_0 \in \mathcal{G}$, the *generating kernel*

$$(3.1) \quad K(p, p_0) := \operatorname{Re} \langle \psi_p, \psi_{p_0} \rangle_{L^2} = \operatorname{Re} \left(\int_{\mathbb{R}^2} \psi_p(x, y) \overline{\psi_{p_0}(x, y)} dx dy \right).$$

This kernel expresses the strength of *correlation* between the RPs of two cells, represented by the points p and p_0 of the feature space. It extends to a general family of filters the idea of the reproducing kernel associated to a family of wavelets ([27], [10]). Now, it is not restrictive to assume that the filters are normalised to have squared L^2 -norm equal to some $\eta > 0$. Under this assumption, we define the *kernel distance*

$$(3.2) \quad d^2(p, p_0) = 2(\eta - K(p, p_0)).$$

Note that d^2 coincides with the squared L^2 distance between the functions ψ_p and ψ_{p_0} . Indeed, $\|\psi_p - \psi_{p_0}\|_{L^2}^2$ can be rewritten as

$$\|\psi_p\|_{L^2}^2 + \|\psi_{p_0}\|_{L^2}^2 - 2\operatorname{Re} \langle \psi_p, \psi_{p_0} \rangle_{L^2}.$$

The generator K and the kernel distance d have a local sense. Indeed, the filters typically have a very localised support and it does not make much sense to compute L^2 scalar products between them if they are not sufficiently close together in the space domain. Moreover, the shape of the specific filters taken into consideration may bring one to introduce some restriction on which filters can directly be influenced by one another. This corresponds to defining around each point $p_0 \in \mathcal{G}$ a local distance function defined on a *patch*, which we shall call $\mathcal{P}(p_0)$, and to gluing all these local distances together to obtain a global distance function

$$(3.3) \quad \tilde{d}(p, p_0) = \inf \left\{ \sum_{j=1}^N d(q_{j-1}, q_j) : N \in \mathbb{N}, q_0 = p_0, q_N = p, q_j \in \mathcal{P}(q_{j-1}) \forall j \right\}.$$

Under a non-degeneracy condition on the definition of such patches, this is still well-defined as a distance function (see [21] for more details).

3.2. Propagation by repeated applications of K . A cortex model must be able to explain not only the action of RPs but also contextual influences and the emergence of association fields. The main existing differential models define on the feature space a Lie group structure, on which the horizontal connectivity is described by means of a diffusion equation expressed through second order operators associated to an invariant sub-Riemannian metric (see e.g. [8]). By contrast, in the present model the local geometry of the cortical space is determined by the receptive profiles of the neurons themselves, through a generating kernel which expresses the reciprocal influences between simple cells with overlapping RFs. The long-range connectivity is then described by iterating the action of this kernel.

It is important to remark that the horizontal connections take place in V1 layer 2/3, which is composed of phase-invariant complex cells. Note that

$$K(p, p_0) = \text{Re}\langle\psi_p, \psi_{p_0}\rangle_{L^2} = \langle\text{Re}\psi_p, \text{Re}\psi_{p_0}\rangle_{L^2} + \langle\text{Im}\psi_p, \text{Im}\psi_{p_0}\rangle_{L^2},$$

which for $p = p_0$ reads

$$K(p, p) = \|\text{Re}\psi_p\|_{L^2}^2 + \|\text{Im}\psi_p\|_{L^2}^2.$$

This recalls the classical energy model for V1 complex cells. In the case of Gabor filters, this is indeed the square sum of a quadrature pair of filters, since the real and imaginary parts of $\psi_{x,y,\theta,\sigma}$ show the same orientation and scale but are shifted in phase of 90° .

Now, how does the activity spread to reach neurons with widely separated receptive fields? Consider the generating kernel K computed around a point p_0 , i.e.

$$(3.4) \quad p \mapsto K(p, p_0) := K_1^{p_0}(p),$$

and define

$$K_2^{p_0}(p) := \int_{\mathcal{G}} K(p, q)h(K_1^{p_0}(q))d\mu(q),$$

where h is a nonlinear *activation function*, essentially implementing the principle of non-maxima suppression. This allows to include in the description of the propagation of neural activity a joint influence of local connections within the same hypercolumn and long-range horizontal connections (as in [5], [6] or [8]). We iterate this procedure, thus defining

$$K_{n+1}^{p_0}(p) := \int_{\mathcal{G}} K(p, q)h(K_n^{p_0}(q))d\mu(q).$$

Here, μ is a suitable measure defined on \mathcal{G} (see [21]). Note that, at each step, the support of the kernel widens.

This idea can be applied to model the response of the layers of V1 to any visual stimulus I applied to the retina, taking into account the contextual influences. In this case, the information reaching the cortex through the visual pathways is given by the function I_0 of the cortical coordinates

$$I_0(p) = \int I(x, y)\psi_p(x, y)dxdy.$$

The action of the generator K on the image is then expressed by

$$I_1(p) := \int_{\mathcal{G}} K(p, q)h(I_0(q))d\mu(q),$$

and at the n -th step we get

$$I_n(p) := \int_{\mathcal{G}} K(p, q)h(I_{n-1}(q))d\mu(q).$$

In our parallel work [21] we constructed a diffusion process on the feature space, equipped with a suitable measure linked with the distance d , to describe the propagation along the connectivity. Under certain conditions ([32],[31]), this process can be approximated by updating the initial datum through repeated integrations of the initial datum against the kernel K . See [21] for further details. This remark highlights a link between our kernel-based model and the diffusion-based differential models cited before, showing that these two approaches can actually coexist.

4. RESULTS

In this section we show, through some numerical simulations, the geometrical properties of the connectivity kernels obtained by applying our model to some different banks of filters. First, we present the classical case of a family of Gabor filters (of fixed scale). We then take into account the spatiotemporal behaviour of the receptive fields by considering a family of three-dimensional Gabor filters including a time parameter. Finally, we show that it is still possible to recover a similar connectivity pattern starting from a family of filters obtained through a learning algorithm, whose parameterization carries no a priori geometric information.

4.1. Gabor filters. The first example we propose is that of a bank of Gabor filters. Its general element reads:

$$(4.1) \quad \psi_{x,y,\theta}(u,v) = \exp\left(\frac{2\pi i X}{\lambda}\right) \exp\left(-\frac{X^2 + Y^2}{2\sigma^2}\right),$$

with

$$\begin{cases} X = (u - x) \cos \theta + (v - y) \sin \theta \\ Y = -(u - x) \sin \theta + (v - y) \cos \theta. \end{cases}$$

Denote $p = (x, y, \theta)$ and $p_0 = (x_0, y_0, \theta_0)$. We have:

$$K(p, 0) = \sigma^2 \pi \exp\left(-\frac{x^2}{4\sigma^2} - \frac{y^2}{4\sigma^2} - \frac{2\sigma^2 \pi^2 (1 - \cos \theta)}{\lambda^2}\right) \cos\left(\pi \frac{x(1 + \cos \theta) + y \sin \theta}{\lambda}\right).$$

The distance induced by K is given by:

$$(4.2) \quad d^2(p, 0) = 2\sigma^2 \pi - 2K(p, 0).$$

The explicit expression for $K(p, p_0)$ for $p_0 \neq 0$ can be obtained from the one for $K(p, 0)$ thanks to the following property.

$$K(x, y, \theta; x_0, y_0, \theta_0) = K(a, b, \delta; 0, 0, 0),$$

with

$$(4.3) \quad \begin{cases} a = (x - x_0) \cos \theta_0 + (y - y_0) \sin \theta_0; \\ b = -(x - x_0) \sin \theta_0 + (y - y_0) \cos \theta_0; \\ \delta = \theta - \theta_0. \end{cases}$$

In [21], we show that in the Gabor case d is locally equivalent to a Riemannian distance, and that such a metric turns out to be a Riemannian approximation to the sub-Riemannian structure defined in [8] on $\mathbb{R}^2 \times S^1$.

As anticipated in the general description above, in order to have a meaningful global distance on the whole feature space it might be preferable to adjust d through a local glueing. In the case of Gabor filters, the level sets of the kernel K (or equivalently, of the distance d) are in general not connected. This is due to the oscillations of the periodic factor: a possible way to keep track more clearly of the meaningful information is to consider only the central lobe.

Consider the following *patch* around each point $p_0 = (x_0, y_0, \theta_0) \in \mathbb{R}^2 \times S^1$:

$$\mathcal{P}(p_0) := \{p = (x, y, \theta) : |a(1 + \cos \delta) + b \sin \delta| < \lambda\},$$

with a, b, δ as in (4.3). This provides an example of adjustment that can be introduced on the original distance function in order to define, if needed, some restriction on which filters are influenced by one another. At this point we can define our metric structure locally, i.e. truncate

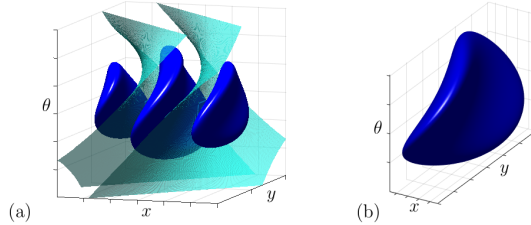


FIGURE 4.1. (a) In dark blue, a level set of $K((x, y, \theta), (0, 0, 0))$. The patch $\mathcal{P}(0, 0, 0)$ is the area between the two surfaces displayed in light blue. (b) The same level set, after truncating. Here, $\lambda = 1$.

the distance function by defining it on $\mathcal{P}(p_0)$ around each point p_0 (see Figure 4.1), and then glue these functions together as in Equation (3.3) to obtain a new global structure.

Since the feature space is of the form *position* \times *orientation*, it is possible to display a visualization on the retinal plane of the generator K around a point. For a fixed point $(x_0, y_0, \theta_0) \in \mathcal{G}$, the function (3.4) reads:

$$(x, y, f) \mapsto K((x, y, \theta), (x_0, y_0, \theta_0)).$$

By taking the maximum in the variable θ and projecting onto the (x, y) plane, we obtain a 2D

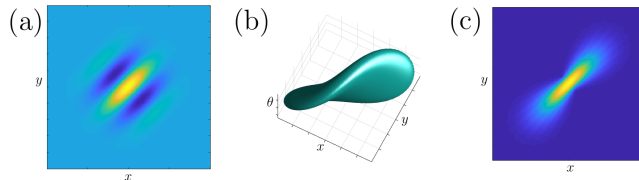


FIGURE 4.2. The behaviour of $(x, y, \theta) \mapsto K((x, y, \theta), (0, 0, \frac{\pi}{4}))$ in the case of Gabor filters. In particular, (a) The receptive profile ψ_{p_0} corresponding to $p_0 = (0, 0, \frac{\pi}{4})$. (b) a level set in $\mathbb{R}^2 \times S^1$, (c) the projection on the (x, y) plane obtained taking the maximum in θ .

function concentrated around (x_0, y_0) , as displayed in Figure 4.2(c).

We now display some stages of the iterative process generated by K , as described in Section 3.2. Figure 4.3 displays the projection onto the retinal plane of the connectivity kernel around $\psi_{0,0,0}$, resulting from three steps of the iterative process. For $n = 1, 2, 3$ the function

$$(4.4) \quad (x, y, \theta) \mapsto h(K_n^{(0,0,0)}(x, y, \theta))$$

was projected on the (x, y) plane by taking the maximum in the variable θ . A further 2D representation of the obtained kernel is displayed, showing at each location (x, y) a tiny Gabor

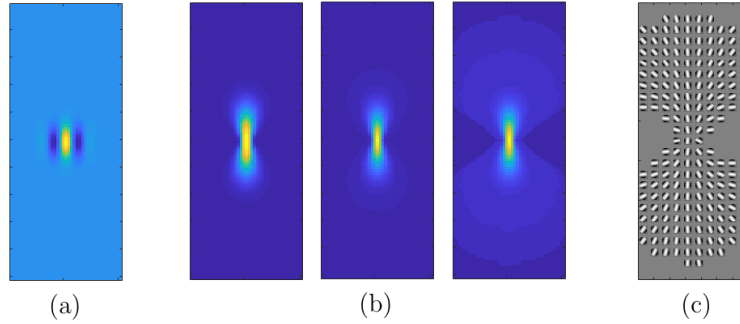


FIGURE 4.3. Development of a connectivity kernel around $(x_0, y_0, \theta_0) = (0, 0, 0)$, obtained through repeated integrations against the generator K . The evolution has been implemented on $] - 2, 2[\times] - 5, 5[\times] - 1.5, 1.5[\subseteq \mathbb{R}^2 \times S^1$, discretized with step 0.1 in x and y and with step 0.15 in θ . Three steps were performed. At each step, the kernel obtained was truncated as explained in Section 2.1.1, and a sigmoidal activation function was then applied. The resulting function $u(x, y, \theta)$ was then projected on the image plane by taking the maximum in the variable θ . The pictures show: (a) The Gabor filter $\psi_{0,0,0}$ (real part). (b) The projection on the (x, y) -plane of the 3D function obtained at each of the three steps. (c) For each (x, y) , the value $\bar{\theta} = \arg \max_{\theta} u(x, y, \theta)$ represented through a Gabor filter with orientation $\bar{\theta}$.

filter whose orientation value $\bar{\theta}$ is the one that maximizes the value of the 3D function, i.e.

$$\bar{\theta}(x, y) := \arg \max_{\theta} h(K_3^{(0,0,0)}(x, y, \theta)).$$

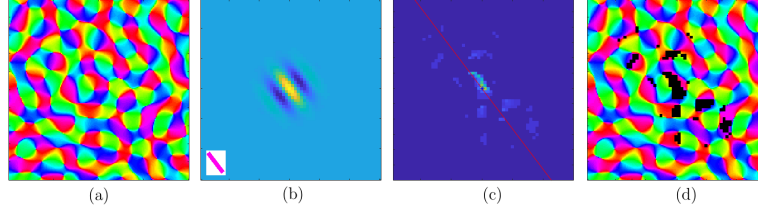


FIGURE 4.4. (a) An orientation map $\theta(x, y)$ generated through superposition of plane waves, as explained in [25]. (b) The filter ψ_{p_0} (real part), where $p_0 = (0, 0, \theta(0, 0))$ is the starting point chosen for the process. In the lower left corner a bar with orientation θ_0 is displayed. Its color is the one corresponding to θ_0 in the pinwheel map. (c) The function $u(x, y, \theta)$ resulting from three steps of evolution through K (with sigmoidal activation at each step), with initial point p_0 , restricted to the pinwheel surface. (d) The values of u exceeding a threshold ($3 \cdot 10^{-5}$), displayed in black onto the orientation map.

Another depiction of the orientation specificity of our connectivity model can be achieved by computing a different projection on the retinal plane: specifically, for each (x, y) we displayed the value of (4.4) at $(x, y, \theta(x, y))$, where the function $\theta(x, y)$ is a simulation of an orientation map. As pointed out in [25], orientation map-like structures can indeed be reproduced as a superposition of plane waves with random phases. Starting from such a map (Figure 4.4(a)), we computed the connectivity kernel around $p_0 = (0, 0, \theta(0, 0))$ and restricted it to the pinwheel surface (Figure 4.4(c-d)). For a comparison, see Figure 4.5, showing the patchy and orientation-

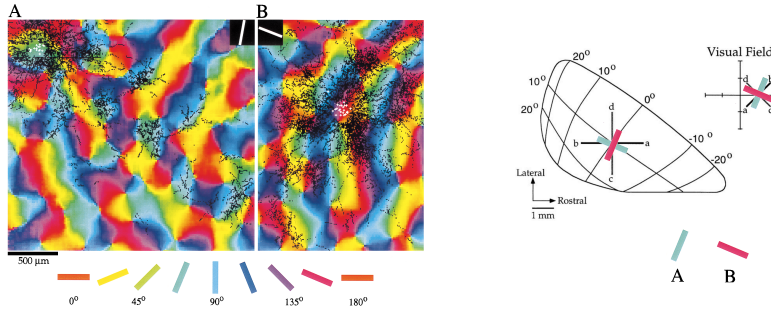


FIGURE 4.5. Top image: distribution of boutons formed after a biocytin injection into a site of tree shrew V1 with a preferred orientation of 80° (A) and 160° (B), displayed over the topographic map of orientation preference. Source: [4]. In order to understand the orientation of this picture, we added (bottom picture) a schematic diagram of the right visual field and left visual cortex of the tree shrew, modified from [4]. The axes ab and cd in the visual field are displayed as they would appear on the cortex. We superposed on the diagram the bars corresponding to the orientations of 80° (A) and 160° (B) in the visual field, and replicated them approximately as they would be mapped on the cortex.

specific distribution of horizontal connections in layer 2/3 of V1 with respect to the topographic map of orientation preference, as measured in [4] in tree shrew V1.

4.2. Spatiotemporal Gabor filters. Let us consider a family of filters still of Gabor type, but taking into account the movement of the stimulus. Cocci et al. [7] fitted the receptive fields of a set of V1 neurons showing velocity-selective behaviours with a three dimensional Gabor model. That is we have, in addition to the two spatial dimensions, a third temporal dimension in the domain of these filters, which in fact form a subset of $L^2(\mathbb{R}^3)$. A convenient visualization of

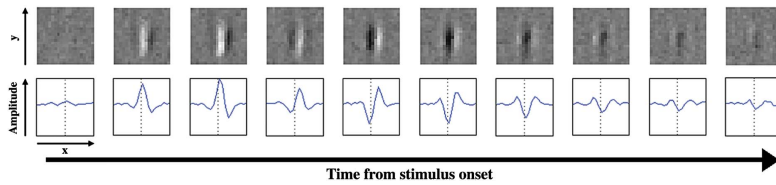


FIGURE 4.6. The time course of the recording of a simple cell's RP. Source: [7].

such filters is as a temporal sequence of spatial maps (see Figure 4.6, taken from [7]). In [3], the authors also develop a differential model of functional architecture based on such 3D Gabor family.

Now, in order to maintain the notations as similar as possible to the one that we used for 2D Gabor filters, we shall write the general *inseparable* element of the family of filters as

$$\psi_{x,y,\theta,t,\alpha}(u,v,s) = \exp\left(-2\pi i \left(\frac{X}{\lambda} + \alpha(s-t)\right)\right) \exp\left(-\frac{X^2 + Y^2}{2\sigma^2} - \frac{(s-t)^2}{2\beta^2}\right),$$

(4.5)

where

$$\begin{cases} X = (u-x)\cos\theta + (v-y)\sin\theta \\ Y = -(u-x)\sin\theta + (v-y)\cos\theta. \end{cases}$$

The set of filters is indexed by the position $(x, y) \in \mathbb{R}^2$, the orientation $\theta \in S^1$, the time $t \in \mathbb{R}^+$ at which the response of the filter is maximum, and the velocity $\alpha \in \mathbb{R}$. Parameters λ and β are fixed.

Let us compute the generating kernel K in this setting. The feature space in this case is $\mathbb{R}^2 \times S^1 \times \mathbb{R} \times \mathbb{R}$. We shall compute $K((x, y, \theta, t, \alpha), (x_0, y_0, \theta_0, t_0, \alpha_0))$ with $t = t_0$: this means considering two cells whose activation peaks at the same time. In other words, we fix t and we take $\mathcal{G} = \mathbb{R}^2 \times S^1 \times \mathbb{R}$ as our feature space. We restrict to this case in order to be able to better interpret the results in terms of the orientation and velocity parameters. Denote $p = (x, y, \theta, \alpha)$ and $p_0 = (x_0, y_0, \theta_0, \alpha_0)$. We obtain the following expression.

$$K(p, p_0) = K^{\text{spatial}}((x, y, \theta), (x_0, y_0, \theta_0)) \cdot \beta^2 \sqrt{\pi} \exp\left(-\frac{\beta^2(\alpha - \alpha_0)^2}{4}\right),$$

where K^{spatial} denotes the generator obtained in the time-independent case discussed above. Through repeated integrations against K , we obtain the connectivity kernels $K_n^{(x_0, y_0, \theta_0, \alpha_0)}$ associated to this family of filters. Since we are considering a 4-dimensional feature space, we

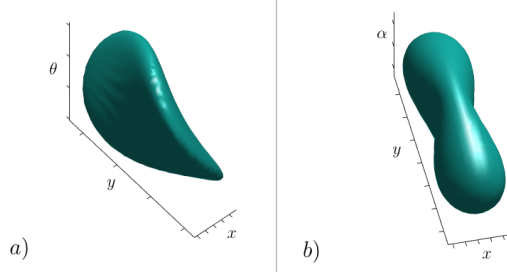


FIGURE 4.7. Visualizations of the spatiotemporal connectivity kernel computed around the point $(x_0, y_0, \theta_0, \alpha_0) = (0, 0, 0, 0)$. a) A level set of its projection onto the (x, y, θ) space, obtained by taking the maximum in α . b) A level set of its projection onto the (x, y, α) space, obtained by taking the maximum in θ .

visualize the kernel by projecting it onto the 3-dimensional spaces $\mathbb{R}^2 \times S^1$ (position and orientation) and $\mathbb{R}^2 \times \mathbb{R}$ (position and velocity). Figure 4.7 displays the kernel around $p_0 = (0, 0, 0, 0)$ projected (a) onto $\mathbb{R}^2 \times S^1$ by taking the maximum in the variable α , and (b) onto $\mathbb{R}^2 \times \mathbb{R}$ by taking the maximum in the variable θ .

Note that the filters $\psi_{x,y,\theta,t,\alpha}$ represent cells that respond maximally to only one direction of movement (depending on the sign of α): such profiles are called *inseparable*. However, there exist also cells which are equally sensitive to both directions, whose profiles are called *separable* (since they can be obtained by the product of two *real* functions of space and time respectively), as well as cells sensitive to both directions but to a different extent. The family of all these profiles can be obtained through weighted sums of inseparable profiles [7]:

$$\psi_{x,y,\theta,t,\alpha}^C(u, v, s) = C\psi_{x,y,\theta,t,\alpha}(u, v, s) + (1 - C)\psi_{x,y,\theta,t,-\alpha}(u, v, s),$$

(4.6)

where $C \in [0, 1]$ is the *separability index*, weighing the contribute of sensitivity to the two opposite directions of movement, expressed by the velocity parameters α and $-\alpha$. Note that, if we introduce C as a parameter, then α can be taken to be nonnegative as an index.

The generator \tilde{K} for the complete family

$$\{\psi_{x,y,\theta,t,\alpha}^C\}_{x,y,\theta,t,\alpha,C}$$

is easily obtained from the generator K for the inseparable family above. Denote

$$\begin{aligned} q &= (x, y, \theta, t, \alpha, C), \\ q_0 &= (x_0, y_0, \theta_0, t_0, \alpha_0, C_0). \end{aligned}$$

We have:

$$\begin{aligned} \tilde{K}(q, q_0) &= CC_0K(p^+, p_0^+) + C(1 - C_0)K(p^+, p_0^-) \\ &+ (1 - C)C_0K(p^-, p_0^+) + (1 - C)(1 - C_0)K(p^-, p_0^-), \end{aligned}$$

where $p^+ = (x, y, \theta, t, \alpha)$, $p^- = (x, y, \theta, t, -\alpha)$ and p_0^+, p_0^- are defined similarly.

4.3. A family of learned filters. We now provide an example of application of our model to a family of filters with no a priori geometric structures. Specifically, we chose a bank of filters obtained through a learning algorithm first proposed by Olshausen and Field in 1996 [24] in order to find efficient linear codes for natural scenes, as an attempt to understand the response properties of visual neurons in terms of the statistical structure of natural images. Such an algorithm generates a family of localized, oriented, bandpass receptive fields through an unsupervised learning procedure which maximizes sparseness. We used a later version of the

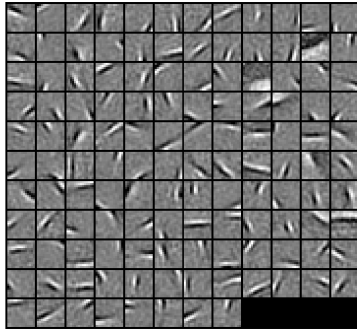


FIGURE 4.8. A bank of 128 filters obtained by training a set of basis functions on natural images (see [24]). The algorithm used is described in [18].

algorithm, provided by Lee et al. in 2007 [18], to generate the bank of 128 filters shown in Figure 4.8.

We then “centered” the support of each filter ψ by identifying the spatial location around which ψ is concentrated and cropping its domain symmetrically around this point to obtain a 11×11 pixel support. The central location was simply chosen to be the point where the function ψ reaches its maximum. To manage the cases in which the maximum point was near the border, we added a 5-pixel padding of zeros around the initial filters before cropping.

At this point, we have a set $\{\psi_f\}_{f=1, \dots, 128}$ of functions centered at zero: by shifting them spatially, we obtain a family of filters $\psi_{x,y,f}$ centered at (x, y) , where $x, y = -N, \dots, N$. Therefore, the feature space in this case can be written as

$$\mathcal{G} = \{-N, \dots, N\}^2 \times \{1, \dots, 128\}.$$

We are now able to compute the generating kernel K . Note that, if we compute the generator associated to the family $\{\psi_{x,y,f}\}_{x,y,f}$ around a point $(0, 0, f_0)$, we can take $N = 10$: indeed, since the filters have a 11×11 support, every time $x > 10$ or $y > 10$ we get

$$K((x, y, f), (0, 0, f_0)) = 0,$$

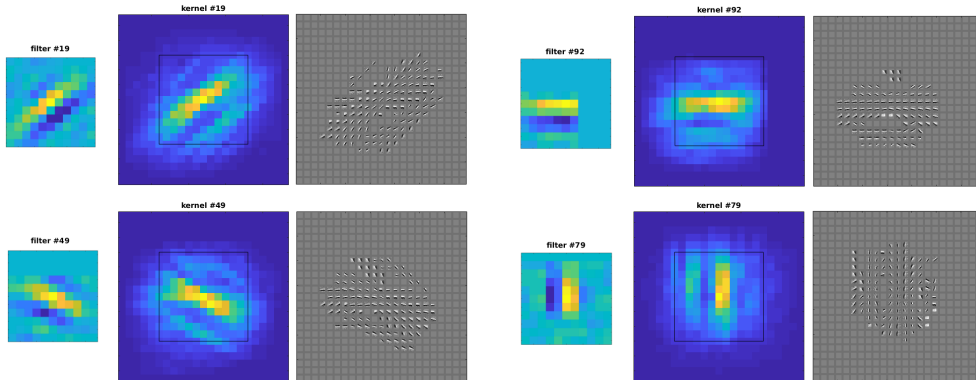


FIGURE 4.9. Visualization of the connectivity kernel around four filters $\psi_{0,0,f_0}$ ($f_0 = 19, 49, 92, 79$). In each of the four cases the image displays, from left to right: the original filter (already cropped around its center); the projection of the kernel on the (x, y) -plane obtained by taking the maximum in the variable f ; the same projection, where instead of the intensity value we displayed at each pixel the filter $\psi_{x,y,f}$ maximizing $K((x, y, f), (0, 0, f_0))$.

because the supports of $\psi_{x,y,f}$ and $\psi_{0,0,f_0}$ do not overlap in this case. See Figure 4.9 for some examples.

Note that in this case we only displayed bidimensional representations of the connectivity kernel. This is still possible since we constructed a parameterization of the family of filters in order to have a feature space of the form *position* \times *features*, so it makes sense to project the results on the (x, y) -plane. However, a meaningful 3D representation of the kernels is no longer possible, since the *feature index* f is simply a parameter and carries no geometric structures.

5. CONCLUSIONS AND FUTURE PROSPECTS

In this paper, we proposed a description of the functional architecture of V1 based on a structure defined directly by the RPs of simple cells. Our construction is very general, since it does not take into account the parameterization of the bank of filters chosen to model the RPs: this makes it possible to define a cortical connectivity even starting from a randomly ordered set of filters resulting e.g. from a regression algorithm, and even in such a case it allows to recover association-field-like patterns.

As was said in Section 2.3, it has been hypothesized [13] that each cortical area might be endowed with an intrinsic connectivity kernel defining a notion analogue to that of V1's association fields. Our model might provide a way to express this kind of interactions in terms of the shape of the RPs of cells different from V1 simple cells, possibly in higher cortical regions.

With a view to future applications, we regard this technique as a possible way to introduce some geometric information on horizontal connections in the context of deep neural networks for artificial vision.

REFERENCES

- [1] A. Angelucci, J. Bullier, *Reaching beyond the classical receptive field of V1 neurons: Horizontal or feedback axons?*, Journal of Physiology Paris, 97, 141-154 (2003).
- [2] F. Anselmi, T. Poggio, *Representation learning in sensory cortex: a theory*, CBMM memo n. 26 (2010).
- [3] D. Barbieri, G. Cocci, G. Citti, A. Sarti, *A cortical-inspired geometry for contour perception and motion integration*, J. Math. Imaging Vis. 49(3), 511-529 (2014).

- [4] W. Bosking, Y. Zhang, B. Schoenfeld, D. Fitzpatrick, *Orientation selectivity and the arrangement of horizontal connections in tree shrew striate cortex*, J Neurosci 17(6), 2112-2127 (1997).
- [5] P. C. Bressloff, J. D. Cowan, *The functional geometry of local and long-range connections in a model of V1*, J. Physiol. Paris, 97, 2-3, 221-236 (2003).
- [6] P.C. Bressloff, J.D. Cowan, M. Golubitsky, P.J. Thomas, M.C. Wiener, *What Geometric Visual Hallucinations Tell Us about the Visual Cortex*, Neural Computation, 14, 473-491 (2002).
- [7] G. Cocci, D. Barbieri, A. Sarti, *Spatiotemporal receptive fields of cells in V1 are optimally shaped for stimulus velocity estimation*, J. Opt. Soc. Am. A, Vol. 29, No. 1 (2012).
- [8] G. Citti, A. Sarti, *A Cortical Based Model of Perceptual Completion in the Roto-Translation Space*, Journal of Mathematical Imaging and Vision archive, Vol. 24, no. 3, 307-326 (2006).
- [9] J. G. Daugman, *Uncertainty relation for resolution in space, spatial frequency, and orientation optimized by two-dimensional visual cortical filters*, J. Opt. Soc. Am. A2, 1160-1169 (1985).
- [10] C.-X. Deng, S. Li, Z.-X. Fu, *The reproducing kernel Hilbert space based on wavelet transform*, Proceedings of the 2010 International Conference on Wavelet Analysis and Pattern Recognition, Qingdao, 370-374 (2010).
- [11] D. J. Field, A. Hayes, R. F. Hess, *Contour integration by the human visual system: evidence for a local association field*, Vision Res 33, 173-193 (1993).
- [12] C. D. Gilbert, A. Das, M. Ito, M. Kapadia, G. Westheimer, *Spatial integration and cortical dynamics*, Proceedings of the National Academy of Sciences USA, Vol. 93, 615-622 (1996).
- [13] C. D. Gilbert, L. Wu, *Top-down influences on visual processing*, Nature Reviews Neuroscience 14, 350-363 (2013).
- [14] S. Grossberg, E. Mingolla, *Neural dynamics of perceptual grouping: Textures, boundaries, and emergent segmentations*, Perception & Psychophysics, 38 (2), 141-171 (1985).
- [15] D. H. Hubel, T. N. Wiesel, *Receptive fields, binocular interaction and functional architecture in the cat visual cortex*, J. Physiol. (London) 160, 106-154 (1962).
- [16] D. H. Hubel, *Eye, brain, and vision*, Henry Holt and Company (1995).
- [17] J. P. Jones, L. A. Palmer, *An evaluation of the two-dimensional Gabor filter model of simple receptive fields in cat striate cortex*, J. Neurophysiol. 58, 1233-1258 (1987).
- [18] H. Lee, A. Battle, R. Raina, A. Y. Ng, *Efficient sparse coding algorithms*, Proceedings of the 19th Annual Conference on Neural Information Processing Systems, Cambridge MA: MIT Press, 801-808 (2007).
- [19] T. S. Lee, *Image Representation Using 2D Gabor Wavelets*, IEEE Transactions on Pattern Analysis and Machine Intelligence, Vol 18, No. 10 (1996).
- [20] L. M. Martinez, J.-M. Alonso, *Complex receptive fields in primary visual cortex*, Neuroscientist, 9(5), 317-331 (2003).
- [21] N. Montobbio, A. Sarti, G. Citti, *A metric model for the functional architecture of the visual cortex* (submitted).
- [22] D. Mumford, *Elastica and computer vision*, in *Algebraic Geometry and its Applications*, 507-518. ed. C. Bajaj, Springer-Verlag (1993).
- [23] H. Neumann, E. Mingolla, *Computational neural models of spatial integration in perceptual grouping*, T. F. Shipley & P. J. Kellman (Eds.), Advances in psychology, 130, *From fragments to objects: Segmentation and grouping in vision*, 353-400 (2001).
- [24] B. A. Olshausen, D. J. Field, *Emergence of simple-cell receptive field properties by learning a sparse code for natural images*, Nature 381, 607-609 (1996).
- [25] J. Petitot, *Neurogéométrie de la vision - Modèles mathématiques et physiques des architectures fonctionnelles*, Éditions de l'École Polytechnique (2008).
- [26] J. Petitot, Y. Tondut, *Vers une neuro-géométrie. Fibrations corticales, structures de contact et contours subjectifs modaux*, Mathématiques, Informatique et Sciences Humaines, vol. 145, 5-101, EHESS, Paris (1999).
- [27] D. Pravica, N. Randriampiry, M. Spurr, *Reproducing kernel bounds for an advanced wavelet frame via the theta function*, Appl. Comput. Harmon. Anal., Vol.33, 79-108 (2012).
- [28] G. Sanguinetti, G. Citti, A. Sarti, *A model of natural image edge co-occurrence in the rototranslation group*, J. Vis. 10(14) (2010).
- [29] A. Sarti, G. Citti, *The constitution of visual perceptual units in the functional architecture of V1*, Journal of Computational Neuroscience, 38(2), 285-300 (2015).
- [30] A. Sarti, G. Citti, J. Petitot, *The symplectic structure of the visual cortex*, Biological Cybernetics, Volume 98, Issue 1, 33-48 (2008).
- [31] K.-T. Sturm, *Diffusion processes and heat kernels on metric spaces*, Ann. Probab. 26(1), 1-55 (1998).
- [32] K.-T. Sturm, *On the geometry defined by Dirichlet forms*, Seminar on Stochastic Analysis, Random Fields and Applications (E. Bolthausen et al., eds.) 231-242. Birkhäuser, Boston (1995).